Frequency measurements of the math xmlns="http://www.w3.org/1998/Math/MathML">mrow>mn>2/mn>msub>mi>ν/mi>mn>3/mn>/msub>msub>mi>A/mi>mn>1/mn>/msub>/mrow>mo>−/mo>msub>mi>ν/mi>mn>3/mn>/msub>/math> band transitions of methane in comb-referenced infrared-infrared double-resonance spectroscopy

Sho Okubo, Hajime Inaba, Shoko Okuda, and Hiroyuki Sasada

Phys. Rev. A **103**, 022809 — Published 10 February 2021

DOI: 10.1103/PhysRevA.103.022809

Precise frequency measurements of the $2\nu_3 A_1$ - ν_3 band transitions of methane in comb-referenced infrared-infrared double-resonance spectroscopy

Sho Okubo and Hajime Inaba
National Metrology Institute of Japan (NMIJ), National Institute of Advanced Industrial Science and Technology (AIST), Tsukuba 305-8563, Japan

Shoko Okuda
Department of Physics, Faculty of Science and Technology, Keio University, Yokohama 223-8522, Japan

Hiroyuki Sasada*
National Metrology Institute of Japan (NMIJ), National Institute of Advanced Industrial Science and Technology (AIST), Tsukuba 305-8563, Japan
Department of Physics, Faculty of Science and Technology, Keio University, Yokohama 223-8522, Japan

(Dated: January 15, 2021)

We carry out infrared-infrared double-resonance spectroscopy of the $2\nu_3 A_1$ - ν_3 band of methane. Ten transitions of Q(1) to Q(4) are observed with an 88.5 THz difference-frequency-generation (DFG) source, while the lower levels are pumped through the ν_3 band transition by another 90.5 THz DFG source phase-locked to an optical frequency comb (OFC). The transition frequencies are determined using an OFC with an uncertainty of 10 kHz, which is an improvement of four orders of magnitude compared with the previous studies.

I. INTRODUCTION

Methane has attracted considerable attention from scientists working in various fields including metrology [1, 2], chemical reaction on potential surfaces [3, 4], the atmospheric science of greenhouse gas [5, 6] and big giant planets [7, 8]. Observations have usually been made using vibration spectroscopy in the mid- and near-infrared regions, and so the precise information provided by high-resolution spectroscopy is eagerly desired in these fields.

Methane belongs to the tetrahedral point group and has four fundamental vibrational modes, ν_1 (87.54 THz, 2920 cm^{-1}), ν_2 (45.97 THz, 1533 cm^{-1}), ν_3 (90.32 THz, 3013 cm^{-1}), and ν_4 (39.30 THz, 1311 cm^{-1}) [9], classified as the A_1 (ν_1 mode), E (ν_2 mode), and F_2 (ν_3 and ν_4 modes) irreducible representations [10]. Because the frequencies have an approximate relation, $\nu_1 \approx 2\nu_2 \approx \nu_3 \approx 2\nu_4$, the vibrational excited states are grouped into polyads; the pentad region (74.6 THz- 95.0 THz, 2490 cm^{-1}- 3170 cm^{-1}), the tetradecad region (150 THz- 187 THz, 5020 cm^{-1}- 6230 cm^{-1}), and the triacontad region (225 THz- 277 THz, 7500 cm^{-1}- 9250 cm^{-1}) [11]. Since the vibrational states in a single polyad are significantly perturbed by each other through vibration and vibration-rotation interactions, global observations and analyses are essential as well as highly precise data.

Double-resonance spectroscopy has proved a powerful tool for investigating atomic and molecular energy levels [12, 13]. Ladder-type double-resonance spectroscopy is particularly useful for probing highly excited states, which are difficult to access through a single-photon transition from thermally populated ground and low-lying excited states. The probe transition can be easily assigned when the pump transition has already been assigned. The transition frequencies can be precisely determined by combining sub-Doppler resolution double-resonance spectroscopy with frequency measurements using an optical frequency comb (OFC). Indeed, the frequencies of the 5P-4D transition of rubidium atoms have been determined by employing optical-optical double-resonance spectroscopy with a typical uncertainty of a few tens of kilohertz [14, 15], while the 5S(ground)-5P transition, whose frequencies have been determined more precisely [16–18], is pumped.

Very recently, OFC Fourier-transform spectroscopy [19] has been applied to the ladder- and lambda-type infrared-infrared double-resonance (IRIRDR) spectroscopy of methane. Ladder-type IRIRDR spectroscopy provides precise transition frequencies and rotational assignments of some vibrational states in the triacontad polyad [20]. The transition frequencies were determined with an average uncertainty of 1.7 MHz, which was mainly limited by the stability of the pump wave frequency.

In this paper, we describe the ladder-type IRIRDR spectroscopy of the $2\nu_3 A_1$ - ν_3 band of methane, where the upper state is a member of the tetradecad polyad. We use two narrow-linewidth continuous-wave difference-frequency-generation (DFG) sources and determine ten transition frequencies of Q(1) to Q(4) using an OFC with an uncertainty of 10 kHz corresponding to a relative uncertainty of 10^{-10}.

Figure 1 shows schematic energy levels associated with the present paper. Black arrows indicate the allowed transitions among the energy levels. Only the F_2 vibrational states are accessible by the electric dipole transition from the ground vibrational state. Since the ν_3 fundamental band is infrared-active, it has been exten-

* sasada@phys.keio.ac.jp

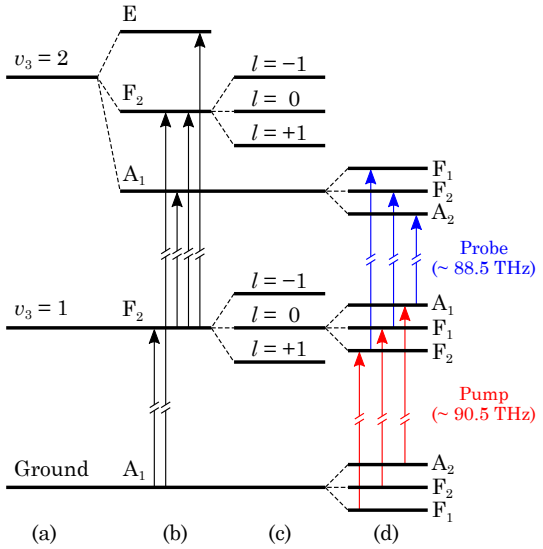

FIG. 1. Schematic energy levels of the low vibrational states of the ν_3 mode with the vibrational quantum number v_3 (a), the vibrational substates (b), the Coriolis sublevels with the vibrational angular momentum quantum number l (c), and the tetrahedral sublevels with a total angular momentum quantum number J of 3 (d). Black arrows indicate the allowed transitions between the vibrational states, and red and blue arrows show the allowed pump and probe vibration-rotation transitions. Energy separations are not scaled.

sively investigated over many years, and comb-referenced sub-Doppler resolution spectroscopy provided 204 transition frequencies with an uncertainty of a few to a few tens of kilohertz [21, 22] and 22 transition frequencies with an average uncertainty of 0.40 MHz [23]. The state with a vibrational quantum number of the ν_3 mode, v_3, of 2 ($v_3 = 2$) in Fig. 1 (a) consists of the A_1 (178.9 THz, 5968 cm^1), F_2 (180.0 THz, 6005 cm^1), and E (181.2 THz, 6044 cm^1) substates in Fig. 1 (b) [24]. Since the $2\nu_3F_2$ band is infrared-active, several transition frequencies have been precisely determined with sub-Doppler resolution spectroscopy [20, 25, 26]. In contrast, the $2\nu_3A_1$ and E bands are not infrared-active but slightly induced by the intensity-borrowing mechanism through certain vibration-rotation interactions. The $2\nu_3A_1$ band is particularly weak as regards single-photon spectroscopy in the 180 THz (6000 cm^1) region [24]. However, as shown in Fig. 1 (b), the $2\nu_3A_1$ - ν_3 and $2\nu_3E$ - ν_3 bands are allowed through the electric dipole transition. Figure 1 (c) and (d) illustrate the Coriolis splitting caused by the vibrational angular momentum quantum number l in the F_2 vibrational substates and the tetrahedral splitting in the vibration-rotation levels in the ground, $v_3 = 1$, and $v_3 = 2A_1$ states, for example, with a total angular momentum quantum number J of 3. The selection rule allows the electric dipole transition between the A_1 and A_2, F_1 and F_2, and E and E vibration-rotation levels. The red and blue arrows in Fig. 1 indicate the allowed pump and probe vibration-rotation transitions of approximately 90.5 THz (3020 cm^1) and 88.5 THz (2950 cm^1), respectively, in the ν_3 and $2\nu_3A_1$ - ν_3 bands. IRIRDR spectroscopy of the $2\nu_3A_1$ - ν_3 and $2\nu_3E$ - ν_3 bands was carried out using pulsed pump and probe waves [27, 28]. However, the spectral resolution of about 4.5 GHz (0.15 cm^1) [28] was too low to resolve the tetrahedral splitting.

II. EXPERIMENTAL

Figure 2 shows our experimental setup. Two near infrared waves of approximately 191.1 THz (6370 cm^1, wavelength of 1.57 μm) and about 281.6 THz (9390 cm^1, wavelength of 1.06 μm) emitted from an extended-cavity laser diode (ECLD) and a Nd:YAG laser, respectively, are converted to a $\sim$90.5 THz (3020 cm^1) wave using DFG for pumping the ν_3 band transitions. Another DFG source for probing the $2\nu_3A_1$ - ν_3 band transitions is described later. The ECLD wave is amplified to 100 mW with an erbium-doped fiber amplifier (EDFA). The Nd:YAG laser wave is also amplified to 200 mW with an ytterbium-doped fiber amplifier (YDFA) and divided into two waves with a power ratio of 7 to 3 in an optical fiber. The former wave is combined with the amplified ECLD wave in a wavelength division multiplexing coupler and is incident on a waveguide-type periodically-polled lithium niobate (PPLN) with a conversion efficiency of about 10 %/W (NTT Electronics), while the latter wave is used for the generation of the probe wave described later. The generated linearly polarized pump wave indicated in red in Fig. 2 has a power level of 1.5 mW and passes twice through a 50 cm long absorption cell, which is fitted with two wedged windows of CaF_2 and filled with naturally abundant methane gas at a pressure of 1.3 Pa. The $1/e^2$ radius of the pump beam is about 0.8 mm along the entire absorption cell.

An optical frequency comb (OFC) used in this study is a homemade erbium-fiber-based mode-locked laser with three branches and with a repetition rate of approximately 100 MHz. These branches are used to phase-lock the waves from the ECLD and the Nd:YAG laser with optical frequencies of ν_{ECLD} and ν_{YAG} to UTC(NMIJ). UTC(NMIJ) is a frequency standard maintained by the National Metrology Institute of Japan by referring to Coordinated Universal Time (UTC), which can be regarded here as equivalent to the primary frequency standard based on the SI second. The design of the OFC system is similar to that used in our past experiment [29]. The ECLD and Nd:YAG laser waves are individually combined with the OFC waves and detected with two InGaAs detectors. The detected beat notes with signed frequencies $\Delta f_{ECLD} = \nu_{ECLD} - \nu_{OFC,ECLD}$ and $\Delta f_{YAG} = \nu_{YAG} - \nu_{OFC,YAG}$ are mixed in an individual phase comparator with a 21.4 MHz sinusoidal signal from two signal generators (SG1, SG2), and the output signal is fed back to the ECLD and Nd:YAG lasers through a proportional-integration (PI) filter, respectively. Here

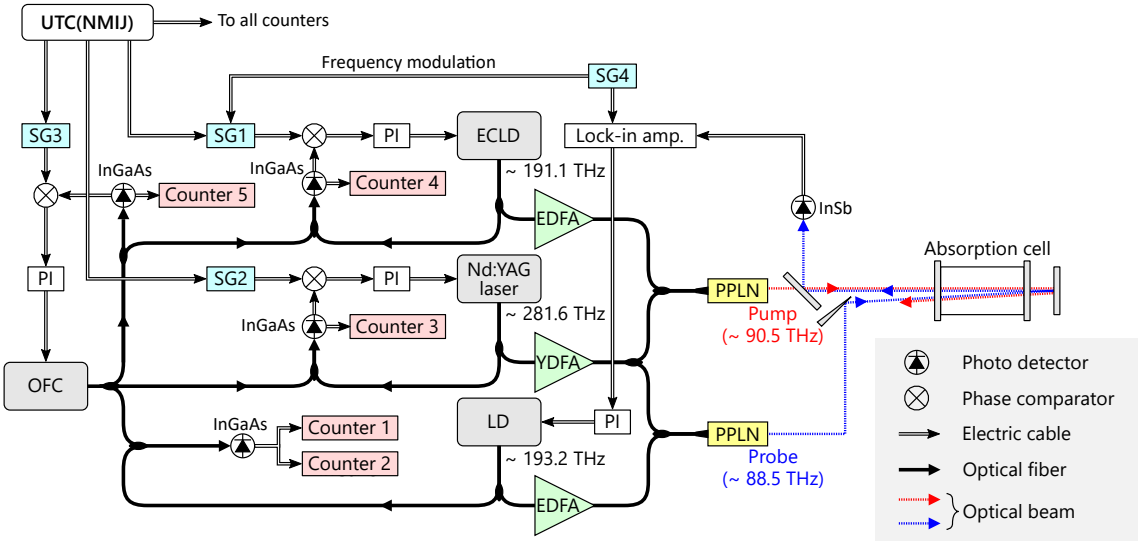

FIG. 2. Experimental setup. The pump and probe waves are shown in red and blue. UTC: Coordinated Universal Time, NMIJ: National Metrology Institute of Japan, SG: signal generator, PI: proportional-integration filter, ECLD: extended-cavity laser diode, EDFA: Er-doped fiber amplifier, YDFA: Yb-doped fiber amplifier, PPLN: periodically-poled lithium niobate, OFC: optical frequency comb, LD: laser diode.

$\nu_{\mathrm{OFC,ECLD}}$ and $\nu_{\mathrm{OFC,YAG}}$, respectively, are the OFC mode frequencies nearest the ECLD and Nd:YAG laser frequencies. Therefore, ν_{ECLD} and ν_{YAG} are phase-locked at optical frequencies by 21.4 MHz higher than that of the nearest individual OFC mode, $\Delta f_{\mathrm{ECLD}} = 21.4\,\mathrm{MHz}$ and $\Delta f_{\mathrm{YAG}} = 21.4\,\mathrm{MHz}$, respectively. Consequently, the frequency of the pump wave, $\nu_{\mathrm{pump}} = \nu_{\mathrm{YAG}} \quad \nu_{\mathrm{ECLD}}$, is an integer multiple of the OFC repetition rate, which is about 99.129 MHz referenced to the signal from a signal generator (SG3). For example, to pump the ν_3 band $\mathrm{Q(3)F_1}$ transition of 90 484 623.067 9 MHz [21], the repetition rate was set at 99.129 074 92 MHz by tuning the frequency of SG3; this repetition frequency is the pump transition frequency divided by the integer 912 796 and rounded to the nearest 10 mHz. The pump wave frequency is thereby 2.8 kHz higher than the pump transition frequency. In the present measurements, the pump wave frequencies are similarly set within 4.5 kHz from the pump transition frequencies [21]. The phase-locked ECLD wave is further frequency-modulated by modulating the offset-frequency Δf_{ECLD} of 21.4 MHz [30]. The modulation signal is provided by another signal generator (SG4) with a modulation frequency of 100 kHz and a peak-to-peak frequency-modulation amplitude of 300 kHz. Since the servo control of the ECLD responds sufficiently fast to the 100 kHz modulation, the pump wave is frequency modulated in the same manner as the modulation signal.

A $\sim$88.5 THz (2950 cm^1) probe wave for IRIRDR spectroscopy is delivered from another DFG source using two waves from a narrow-linewidth $\sim$193.2 THz (6440 cm^1, wavelength 1.55 μm) laser diode (LD, RIO PLANEX) with a frequency of ν_{LD} and the Nd:YAG laser. The LD wave is amplified to the 100 to 250 mW range by another EDFA, combined with 30 % of the amplified Nd:YAG laser wave, and launched into another waveguide-type PPLN similar to that used for the pump wave generation. The generated probe wave shown in blue in Fig. 2 has a power level of typically 0.1 mW and travels through the absorption cell along the pump wave with parallel polarization in the opposite direction. The $1/e^2$ radius of the probe beam is about 0.8 mm along the entire absorption cell. Subsequently, it is partially reflected by a $\mathrm{CaF_2}$ plate and detected with a liquid-nitrogen-cooled InSb detector. The detected signal is phase-sensitively demodulated in a $1f$ mode with a lock-in amplifier at 100 kHz. The demodulated spectral line has a dispersion-like profile and is used as a frequency discriminator to stabilize the probe wave frequency at the center of the IRIRDR spectral line. To accomplish this, the output of the lock-in amplifier is fed back through another PI filter to the injection current level control of the LD. Then the electric signal of the beat note between the LD wave and the nearest OFC mode with a signed frequency of $\Delta f_{\mathrm{LD}} = \nu_{\mathrm{LD}} - \nu_{\mathrm{OFC,LD}}$ passes through an rf filter and enters two separate rf frequency counters (Counters 1 and 2 in Fig. 2) to check the count, where $\nu_{\mathrm{OFC,LD}}$ is the OFC mode frequency nearest the LD frequency. At the same time, three rf frequency counters (Counters 3, 4, and 5) measure the difference frequency between the Nd:YAG laser wave and the nearest OFC mode, Δf_{YAG}, the difference frequency between the ECLD wave and the nearest OFC mode, Δf_{ECLD}, and the OFC repetition rate. These five frequency counters synchronously count the individual frequencies with an averaging time of 1 s for a period of 30 s to 1000 s. The frequency counters and the signal generators (SG1, 2, and 3) are referenced to an atomic clock based on UTC. The rela-

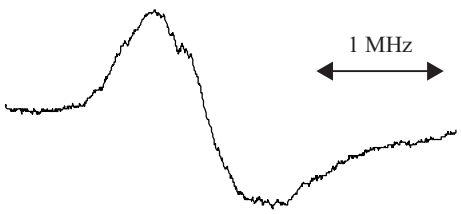

FIG. 3. Observed IRIRDR spectrum of the $2\nu_3$ A_1 - ν_3 band Q(4) A_2 transition.

tive uncertainty of the measured frequencies measured under these conditions using the atomic clock and the optical comb is at worst less than 10^{-13}, which is sufficient low for the present measurement. To determine whether the LD frequency, $\nu_{\rm LD}$, is higher or lower than the nearest OFC mode frequency, $\nu_{\rm OFC,LD}$, we slightly increase the offset frequency of the phase-locking of the ECLD wave, $\Delta f_{\rm ECLD}$. Then the pump wave frequency, $\nu_{\rm pump} = \nu_{\rm YAG}\ \nu_{\rm ECLD}$, decreases and the probe wave frequency, $\nu_{\rm probe} = \nu_{\rm YAG}\ \nu_{\rm LD}$, locked at the center of the IRIRDR signal increases because the pump and probe waves travel in opposite directions. When the beat frequency, $|\Delta f_{\rm LD}|$, increases (decreases), the optical frequency of the LD wave, $\nu_{\rm LD}$, is lower (higher) than that of the nearest OFC mode, $\Delta f_{\rm LD} < 0$ (> 0). The carrier-envelope-offset frequency of the OFC is not controlled because the pump and probe waves are generated in the DFG process.

The approximate optical frequencies of the ECLD, Nd:YAG laser, and LD waves are measured using a wavelength meter (Bristol 621A-NIR, not shown in Fig. 2) to determine the difference between the mode orders of the nearest OFC modes of the laser waves. The nominal relative uncertainty is 2×10^{-7} corresponding to 56 MHz for the Nd:YAG laser wave and 38 MHz for ECLD and LD waves. These values are smaller than the OFC repetition rate of about 99.129 MHz. To ensure the mode order difference of the OFC, the probe transition frequencies are also determined with another repetition rate of about 99.994 MHz; both results are consistent within the experimental uncertainties.

III. RESULTS

Figure 3 shows the spectrum of the $2\nu_3 A_1$ - ν_3 band Q(4)A_2 transition observed while the ν_3 band Q(4)A_1 transition is pumped. The width of the spectral line between the peak and bottom values of the dispersion-like profile is 0.50 MHz. When we assume that the profile is the first derivative of the Lorentz profile, the half-width at half maximum (HWHM) is 0.43 MHz. The unmodulated linewidth is mainly determined by the sum of the power broadenings of the pump and probe transitions. The Rabi frequencies are estimated to be 0.34 MHz and 0.09 MHz, respectively, when the pump and probe waves have power levels of 1.5 mW and 0.1 mW and beam radii of 0.8 mm, the transition dipole moment of the ν_3 band is 3×10^{-30} C·m ($\sim$ 0.09 Debye) [31], and that of the $2\nu_3 A_1$ - ν_3 band is assumed to be identical. Then the transit-time broadening is about 0.07 MHz [32]. For the ν_3 band $P(7)F_2^{(2)}$ transition of methane, the sub-Doppler resolution saturated spectral line at low pressure has a pressure-broadening coefficient of 60 kHz/Pa (HWHM) [33] caused by a velocity-changing collision, corresponding to the pressure broadening of 0.08 MHz for 1.3 Pa reported in this paper. The frequency-modulation amplitude is 0.30 MHz and comparable to the unmodulated linewidth, where the modulation broadening is not significant but the sensitivity is still high.

The standard deviation of the measured frequency of the beat note between the LD wave and the nearest OFC mode, $\Delta f_{\rm LD}$, is typically a few kilohertz, 1 kHz, and a few hundreds hertz at averaging times of 1 s, 10 s, and 100 s, respectively, for a series of continuous measurements. However, the repeatability with the different series of the measurements is poorer than the standard deviations. The measured beat frequency is sensitive to the offset level of the lock-in amplifier because the LD frequency is locked so that the output level of the lock-in amplifier vanishes. Ideally, IRIRDR signals are not affected by the offset level of the lock-in amplifier because there are no background signals. However, the frequency modulation of the pump wave inevitably causes the residual amplitude modulation (RAM), which induces a shift in the offset level of the lock-in amplifier. Adjustment of the offset level currently limits the repeatability among the series of measurements.

Table I shows the main result. We determined ten transition frequencies in the $2\nu_3 A_1$ - ν_3 band. Table I lists the probe transitions, the determined frequencies, and the uncertainties in parentheses in units of the last digit together with the pump transitions, the frequencies, and the uncertainties [21]. Table II shows the uncertainty budget of the probe transition frequency. The probe wave frequency range is limited to between 88.418 THz (2949.3 $\rm cm^1$) and 88.507 THz (2952.3 $\rm cm^1$) by the tunable ranges of the Nd:YAG laser and the LD. The probe transition frequencies are corrected by considering the slight difference between the pump wave frequency and the pump transition frequency mentioned above. The probe transition frequencies are determined from twelve series of measurements on at least three different days. One series of the measurements typically involves a few hundred continuous one-second measurements. All of the $\Delta f_{\rm LD}$ data are measured by the two counters (Counters 1 and 2) with synchronized timing, and any data with a frequency difference between the two measurements exceeding 0.7 Hz are discarded; in most cases, the difference is less than 5 mHz.

The frequency shifts are investigated by varying the pump wave power and the frequency-modulation ampli-

TABLE I. Measured Frequencies of the $2\nu_3 A_1$ - ν_3 Band Transitions of Methane

Pump transition ν_3 band	Initial level energy divided by h[a,b] (MHz)	Pump transition frequency[b] (MHz) [21]	Probe transition $2\nu_3 A_1$-ν_3 band	Probe transition frequency[b] (MHz) [this work]	Final level energy divided by h[a] (MHz)	Obs. − cal. (MHz)
Q(1) F_1	314 231.917(3)	90 502 080.707 9(21)	Q(1) F_2	88 420 565.920(10)	179 236 878.545	0.000
Q(2) F_2	942 619.090(8)	90 496 856.544 3(20)	Q(2) F_1	88 432 980.296(10)	179 872 455.930	−0.891
Q(2) E	942 611.119(8)	90 495 092.106 1(23)	Q(2) E	88 434 995.358(10)	179 872 698.583	0.891
Q(3) A_2	1 885 040.174(14)	90 493 215.526 8(21)	Q(3) A_1	88 449 013.267(10)	180 827 268.968	−3.320
Q(3) F_2	1 885 000.363(14)	90 488 114.363 3(20)	Q(3) F_1	88 455 587.133(10)	180 828 701.860	7.860
Q(3) F_1	1 884 968.499(14)	90 484 623.067 9(20)	Q(3) F_2	88 460 336.047(10)	180 829 927.614	−4.540
Q(4) F_2	3 141 225.811(20)	90 483 521.742 8(20)	Q(4) F_1	88 481 618.027(10)	182 106 365.581	0.258
Q(4) E	3 141 106.541(20)	90 473 934.281 5(22)	Q(4) E	88 496 445.762(10)	182 111 486.585	−0.612
Q(4) F_1	3 141 066.708(20)	90 471 813.803 4(19)	Q(4) F_2	88 500 849.292(10)	182 113 729.804	−0.041
Q(4) A_1	3 141 010.943(20)	90 468 721.185 7(29)	Q(4) A_2	88 507 067.091(10)	182 116 799.219	0.396

[a] Here h is the Planck constant.
[b] The numbers in parentheses are uncertainties in units of the last digit.

TABLE II. Uncertainty Budget of the Probe Transition Frequency

Effect	Uncertainty
Frequency measurements based on UTC	< 10 Hz
Probe wave frequency locking	10 kHz
Pump frequency	1.9 kHz−2.9 kHz
Power shift	< 1 kHz
Pressure shift	0.73 kHz
Total	10 kHz

tude for the intense $2\nu_3 A_1$ - ν_3 band Q(3)A_1 transition. We find that the offset level of the lock-in amplifier shifts in proportional to the amplitude of the IRIRDR signal, which is varied by the pump wave power and the frequency modulation amplitude. This is why we attribute the frequency shifts to the RAM. Therefore, each time a measurement series starts, we adjust the offset level of the lock-in amplifier so that the output of the lock-in amplifier involving the RAM vanishes in the region far from the IRIRDR spectral line. The sample standard deviations are from 4.0 kHz to 12.4 kHz for the individual probe transitions, and 7.7 kHz for them all. We thereby estimate the uncertainty from the probe wave frequency locking to be 10 kHz, as shown in Table II. The power shift for the ν_3 band P(7) $F_2^{(2)}$ transition of methane [33] is reported to be about 1 kHz for a power density of 1 W/cm^2, which is 13 and 300 times more intense than the present pump and probe waves, respectively. The pressure shift, which is not examined in this work, is estimated to be 0.73 kHz from the pressure shift coefficient of (0.56 ± 1.13) kHz/Pa for the ν_3 band P(7) $F_2^{(2)}$ transition of methane [33], which is considerably smaller than 10 kHz. Therefore, neither the probe transition frequency nor the uncertainty in Table I are corrected by the power shift and pressure shift. The uncertainty of the probe transition frequency is, as shown in Table II, mainly determined by the probe wave frequency locking.

TABLE III. Molecular Constants of the Ground and $v_3 = 2A_1$ States

	Determined values (MHz)	
	Ground State[a]	$v_3 = 2A_1$ State[a]
ν_0	−	178 919 541(16)
B	157 122.614 7(15)	158 593.4(63)
D_s	3.328 554(33)	−36.51(67)
D_t	0.132 941 3(30)	−3.061(45)
$H_s/10^{-5}$	19.098(31)	$6.38(20) \times 10^4$
$H_{4t}/10^{-5}$	−1.6948(54)	$-1.589(24) \times 10^4$
$H_{6t}/10^{-5}$	1.1029(19)	$-7.272(90) \times 10^3$
$L_s/10^{-9}$	−13.45(96)	−
$L_{4t}/10^{-9}$	1.90(23)	−
$L_{6t}/10^{-9}$	−2.73(14)	−
$L_{8t}/10^{-9}$	−1.51(37)	$-1.02(29) \times 10^7$

[a] The numbers in parentheses are uncertainties in units of the last digit.

We have carried out a preliminary analysis of the $v_3 = 2A_1$ vibrational state. The local Hamiltonians H of both the ground and $v_3 = 2A_1$ vibrational states are expressed as

$$\frac{H}{h} = \nu_0 + B\mathbf{J}^2 D_s(\mathbf{J}^2)^2 + H_s(\mathbf{J}^2)^3 + L_s(\mathbf{J}^2)^4 + [D_t + H_{4t}\mathbf{J}^2 + L_{4t}(\mathbf{J}^2)^2]\mathbf{\Omega}_4 + (H_{6t} + L_{6t}\mathbf{J}^2)\mathbf{\Omega}_6 + L_{8t}\mathbf{\Omega}_8, \quad (1)$$

where h, ν_0, B, D_s, H_s, and L_s are the Planck constant, vibrational frequency, rotational constant, scalar centrifugal distortion constant, and the scalar sextic and octic distortion constants. Here $\mathbf{J}$ is a non-dimensional angular momentum operator, $D_t, H_{4t}, H_{6t}, L_{4t}, L_{6t}$, and L_{8t} are tensor distortion constants, and $\mathbf{\Omega}_4, \mathbf{\Omega}_6$, and $\mathbf{\Omega}_8$ are the fourth, sextic, and octic tensor operators. The matrix elements of $\mathbf{\Omega}_4$ and $\mathbf{\Omega}_6$ are given in Ref. [34], and those of $\mathbf{\Omega}_8$ can be found in Ref. [35]. These tensor distortion terms, as shown in Fig. 1 (d), partly lift the rotational degeneracy of the spherical top molecule.

First, ten molecular constants of the ground state, $B, D_{\rm s}, H_{\rm s}, L_{\rm s}, D_{\rm t}, H_{4\rm t}, H_{6\rm t}, L_{4\rm t}, L_{6\rm t}$, and $L_{8\rm t}$ are determined by fitting 23 combination differences of sub-Doppler resolution infrared spectroscopy of the ν_3 band [21, 22, 36, 37] and 9 transition frequencies from the existing microwave data [38–41] associated with the levels of the rotational quantum number J less than or equal to 12 using a weighted nonlinear least-squares method. Table III lists the determined values with the uncertainties in parentheses in units of the last digit. The standard deviation of the fit is 0.021 MHz, and the value of χ^2 is 10.6 for a degree of freedom of 22. Table I shows the initial level energy divided by h and the uncertainty calculated from these molecular constants and the variance-covariance matrix. Table I also shows the final level energy divided by h, which is a sum of the initial level energy divided by h, the pump transition frequency [21], and the probe transition frequency determined in the present study. The rotational levels in the ground and $v_3 = 2\mathrm{A}_1$ vibrational states, as shown in Table I, have a similar tetrahedral level structure, but the order of the energy levels is opposite.

Subsequently, eight molecular constants of the $v_3 = 2\mathrm{A}_1$ vibrational state, $\nu_0, B, D_{\rm s}, H_{\rm s}, D_{\rm t}, H_{4\rm t}, H_{6\rm t}$, and $L_{8\rm t}$ are determined by fitting the ten final level energies using an equally-weighed nonlinear least-squares method. Table III lists the determined values together with the uncertainty in the parenthesis in unit of the last digit. The standard deviation of the fit is 6.9 MHz, which is considerably larger than the uncertainties of the final level energy determined by the uncertainties of the pump and probe transition frequencies and the uncertainty of the initial level energy. The residuals of the fit are listed as obs. cal. in the last column of Table I . The sum over the transitions with common J vanishes because the number of scalar constants, $\nu_0, B, D_{\rm s}$, and $H_{\rm s}$, is equal to the independent data number, the Q(1) to Q(4) transitions. It is noted that the rotational constant of the $v_3 = 2\mathrm{A}_1$ vibrational substate is 0.91 % larger than that of the ground vibrational state, as pointed out in Ref. [28], and that the value of $D_{\rm s}$ is negative. The signs of $D_{\rm t}$s are opposite for these states, as recognized in Ref. [24].

It is evident that the local Hamiltonian of Eq.(1) for the $v_3 = 2\mathrm{A}_1$ substate is insufficiently accurate to reproduce the final level energies within the experimental uncertainty even though a similar Hamiltonian for the ground state is able to reproduce the measured combination differences and the microwave frequencies. In Table III, the molecular constants in the ground state converge rapidly as the power of **J**: The ratios of $D_{\rm s}$, $H_{\rm s}$, and $L_{\rm s}$ to B are approximately 10^{-5}, 10^{-10}, and 10^{-14}. In contrast, the corresponding ratios are 10^{-4}, 10^{-7}, and 10^{-7} in the $v_3 = 2\mathrm{A}_1$ substate. This suggests that a global analysis involving the interaction with the other vibrational states is required rather than a local analysis. In general, vibration-rotation interactions in highly excited vibrational states are more significant than in low-lying vibrational states. This is, in particular, the case for methane. The $v_3 = 2\mathrm{A}_1$ substate in the tetradecad polyad is significantly perturbed from the other members of the polyad. An understanding of the $v_3 = 2\mathrm{A}_1$ substate requires more extensive measurements of the tetradecad polyad [42].

IV. CONCLUSION

We carried out precise IRIRDR spectroscopy of the $2\nu_3\mathrm{A}_1$-ν_3 band of methane. Ten transition frequencies were determined with 10 kHz uncertainty using an OFC. The precision bears comparison with single-photon spectroscopy of the molecular transitions from the ground and low-lying vibrational states.

ACKNOWLEDGMENTS

We are grateful to JST, ERATO MINOSHIMA Intelligent Optical Synthesizer Project for partial financial support at the earliest stage of this study.

[1] E. Kovalchuk, T. Schuldt, and A. Peters, Opt. Lett. **30**, 3141 (2005).
[2] M. A. Gubin, A. N. Kireev, A. V. Konyashchenko, P. G. Kryukov, A. S. Shelkovnikov, A. Tausenev, and D. A. Tyurikov, Appl. Phys. B **95**, 661 (2009).
[3] S. Peyerimhoff, M. Lewerenz, and M. Quack, Chem. Phys. Lett. **109**, 563 (1984).
[4] X.-G. Wang and T. Carrington, J. Chem. Phys. **119**, 101 (2003).
[5] M. A. K. Khalil, Annu. Rev. Energy Environ. **24**, 645 (1999).
[6] H. Chen, J. Winderlich, C. Gerbig, A. Hoefer, C. W. Rella, E. R. Crosson, A. D. Van Pelt, J. Steinbach, O. Kolle, V. Beck, B. C. Daube, E. W. Gottlieb, V. Y. Chow, G. W. Santoni, S. Wofsy, E. Charles Kovalchuk, T. Schuldt, and A. Peters, Atmos. Meas. Tech. **3**, 375 (2010).
[7] P. Irwin, K. Sihra, N. Bowles, F. Taylor, and S. Calcutt, Icarus **176**, 255 (2005).
[8] L. Sromovsky and P. Fry, Icarus **193**, 252 (2008).
[9] S. Albert, S. Bauerecker, V. Boudon, L. Brown, J.-P. Champion, M. Lote, A. Nikitin, and M. Quack, Chem. Phys. **356**, 131 (2009).
[10] G. Herzberg, *Molecular spectra and molecular structure: Infrared and Raman of Polyatomic Molecules* (D. van Nostrand Co., 1950).
[11] O. N. Ulenikov, E. S. Bekhtereva, S. Albert, S. Bauerecker, H. M. Niederer, and M. Quack, J. Chem.

Phys. **141**, 234302 (2014).
[12] K. Shimoda, Double-resonance spectroscopy of molecules by means of lasers (Springer-Verlag GmbH, 1976) Chap. 3, pp. 197–252.
[13] W. Demtröder, *Laser Spectroscopy*, 4th ed. (Springer Berlin Heidelberg, Berlin New York, 2008).
[14] W.-K. Lee, H. S. Moon, and H. S. Suh, Opt. Lett. **32**, 2810 (2007).
[15] W.-K. Lee and H. S. Moon, Phys. Rev. A **92**, 012501 (2015).
[16] J. Ye, S. Swartz, P. Jungner, and J. L. Hall, Opt. Lett. **21**, 1280 (1996).
[17] G. P. Barwood, P. Gill, and W. R. C. Rowley, Appl. Phys. B **53**, 142 (1991).
[18] A. Banerjee, D. Das, and V. Natarajan, Opt. Lett. **28**, 1579 (2003).
[19] P. Maslowski, K. F. Lee, A. C. Johansson, A. Khodabakhsh, G. Kowzan, L. Rutkowski, A. A. Mills, C. Mohr, J. Jiang, M. E. Fermann, and A. Foltynowicz, Phys. Rev. A **93**, 021802 (2016).
[20] A. Foltynowicz, L. Rutkowski, I. Silander, A. C. Johansson, V. S. de Oliveira, O. Axner, G. Soboń, T. Martynkien, P. Mergo, and K. K. Lehmann, (2020), arXiv:2001.08781.
[21] S. Okubo, H. Nakayama, K. Iwakuni, H. Inaba, and H. Sasada, Opt. Express **19**, 23878 (2011).
[22] M. Abe, K. Iwakuni, S. Okubo, and H. Sasada, J. Opt. Soc. Am. B **30**, 1027 (2013).
[23] P. A. Kocheril, C. R. Markus, A. M. Esposito, A. W. Schrader, T. S. Dieter, and B. J. McCall, J. Quant. Spectrosc. Radiat. Transf. **215**, 9 (2018).
[24] A. Nikitin, I. Chizhmakova, M. Rey, S. Tashkun, S. Kassi, D. Mondelain, A. Campargue, and V. Tyuterev, J. Quant. Spectrosc. Radiat. Transfer **203**, 341 (2017).
[25] C. Ishibashi, M. Kourogi, K. Imai, B. Widiyatmoko, A. Onae, and H. Sasada, Opt. Commun. **161**, 223 (1999).
[26] H. Lin, L. Yang, X. J. Feng, and J. T. Zhang, Phys. Rev. Lett. **122**, 013002 (2019).
[27] A. D. Martino, R. Frey, and F. Pradere, Chem. Phys. Lett. **95**, 200 (1983).
[28] A. D. Martino, R. Frey, and F. Pradere, Chem. Phys. Lett. **100**, 329 (1983).
[29] Y. Nakajima, H. Inaba, K. Hosaka, K. Minoshima, A. Onae, M. Yasuda, T. Kohno, S. Kawato, T. Kobayashi, T. Katsuyama, and F.-L. Hong, Opt. Express **18**, 1667 (2010).
[30] K. Iwakuni, S. Okubo, and H. Sasada, Opt. Express **21**, 14832 (2013).
[31] L. Fjard, J. Champion, J. Jouvard, L. Brown, and A. Pine, J. Mol. Spectrosc. **201**, 83 (2000).
[32] M. Abe, K. Iwakuni, S. Okubo, and H. Sasada, Opt. Lett. **39**, 5277 (2014).
[33] R. L. Barger and J. L. Hall, Phys. Rev. Lett. **22**, 4 (1969).
[34] S. M. Kirschner and J. K. Watson, J. Mol. Spectrosc. **47**, 347 (1973).
[35] I. Ozier, J. Mol. Spectrosc. **53**, 336 (1974).
[36] S. Okuda, Bachelor's thesis, Keio University (2015).
[37] Y. Kobayashi, Bachelor's thesis, Keio University (2017).
[38] R. Curl, T. Oka, and D. Smith, J. Mol. Spectrosc. **46**, 518 (1973).
[39] R. Curl, J. Mol. Spectrosc. **48**, 165 (1973).
[40] W. M. Itano and I. Ozier, J. Chem. Phys. **72**, 3700 (1980).
[41] M. Oldani, M. Andrist, A. Bauder, and A. Robiette, J. Mol. Spectrosc. **110**, 93 (1985).
[42] A. V. Nikitin, V. Boudon, C. Wenger, S. Albert, L. R. Brown, S. Bauerecker, and M. Quack, Phys. Chem. Chem. Phys. **15**, 10071 (2013).